

Analyses of multi-pion Bose-Einstein correlations for granular sources with coherent pion-emission droplets

Ghulam Bary¹, Wei-Ning Zhang^{1,2*}, Peng Ru³, Jing Yang⁴

¹*School of Physics, Dalian University of Technology, Dalian, 116024, China*

²*School of Physics, Harbin Institute of Technology, Harbin, 150006, China*

³*Institute of Quantum Matter, South China Normal University, Guangzhou, 510006, China*

⁴*School of Physics, Changchun Normal University, Changchun, 130032, China*

The ALICE Collaboration measure the three- and four-pion Bose-Einstein correlations (BECs) in Pb-Pb collisions at the Large Hadron Collider (LHC). It is speculated that the significant suppressions of multi-pion BECs are due to a considerable degree of coherent pion emission in the collisions. In this paper, we study the multi-pion BEC functions in a granular source model with coherent pion-emission droplets. We find that the intercepts of multi-pion correlation functions at the relative momenta near zero are sensitive to droplet number in the granular source. They decrease with decreasing droplet number. The three-pion correlation functions for the evolving granular sources with momentum-dependent partially coherent pion-emission droplets are in basic agreement with the experimental data in Pb-Pb collisions at $\sqrt{s_{NN}} = 2.76$ TeV at the LHC. However, the model results of four-pion correlation function are inconsistent with the experimental data. The investigations of the normalized multi-pion correlation functions of the granular sources indicate that there is an interesting enhancement of the normalized four-pion correlation function in moderate relative-momentum region.

PACS numbers: 25.75.-q, 25.75.Gz

I. INTRODUCTION

Identical pion intensity correlations (Bose-Einstein correlations, BECs) are important observables in high-energy heavy-ion collisions [1–6]. Because the multiplicity of identical pions in heavy-ion collisions at the Large Hadron Collider (LHC) is very high, multi-pion BEC analyses with high statistic accuracy are available [7, 8]. Recently, the ALICE Collaboration measured significant suppressions of three- and four-pion BECs in Pb-Pb collisions at $\sqrt{s_{NN}} = 2.76$ TeV at the LHC [7, 8], which indicates that there may exist a considerable coherence degree for the particle-emitting sources produced in the collisions [7–11].

Analyses of multi-pion BECs can provide more information of the particle-emitting sources compared with two-pion interferometry [4, 5, 7–26]. In particular, multi-pion BECs are sensitive to source coherence [9–12, 20]. In Refs. [10, 11], we investigated three- and four-pion BECs for a spherical evolving source of pion gas with identical boson condensation. However, the particle-emitting sources produced in relativistic heavy-ion collisions are anisotropic in space and may have complex structure. It is of interest to explain the experimental measurements of multi-pion BEC suppressions at the LHC based on a more realistic model that can also explain the other observables in the collisions.

On an event-by-event basis, the initial systems produced in relativistic heavy-ion collisions are highly fluctuated in space. This initial fluctuation may lead to an

inhomogeneous particle-emitting source, in which there are hot spots and cold valleys. In Refs. [27–30], a granular source model was proposed and developed by Zhang et al. to explain the experimental results of two-pion interferometry at the Relativistic Heavy Ion Collider (RHIC) and LHC [31–33]. In Refs. [34–36], the granular source model was used to systemically study the pion transverse-momentum spectra, elliptic flows, and two-pion BECs in heavy-ion collisions at the RHIC and LHC. The granular source model can reproduce the experimental data of pion transverse-momentum spectrum, elliptic flow, and two-pion interferometry radii [34–36]. Considering identical pions are emitted from the droplets in the granular source model and the droplet radii are much smaller than the source size, the pion emission from one droplet is perhaps coherent in the case of high pion event multiplicity due to the condensation of identical bosons [10, 11, 41, 42].

In this work, we consider a granular source with coherent pion-emission droplets. The droplets in the granular source move with anisotropic velocities and evolve in viscous hydrodynamics, as described in Ref. [36]. However, identical pion emissions from one droplet are assumed to be completely or partially coherent. We investigate multi-pion BECs in the granular source model with coherent pion-emission droplets. The normalized three- and four-pion correlation functions of the granular sources are examined for completely coherent and momentum-dependent partially coherent pion emissions from a droplet.

The rest of this paper is organized as follows. In Sec. II, we examine the three- and four-pion BEC functions of a static granular source with coherent pion-emission droplets. In Sec. III, we investigate the three- and four-

*wnzhang@dlut.edu.cn

pion BECs in the granular source model in which the droplets evolve in viscous hydrodynamics. We also investigate the normalized multi-pion correlation functions of the evolving granular sources in this section. Finally, we give a summary and discussion in Sec. IV.

II. MULTI-PION BECS OF STATIC GRANULAR SOURCES

We first consider a static granular source in which identical pions are emitted from separated droplets. The spa-

tial distribution of the emitting points in each droplet is assumed with a Gaussian distribution $\sim e^{r^2/(2r_d^2)}$, and the droplet centers R_j ($j = 1, 2, \dots, n$) distribute in the granular source with a Gaussian distribution $\sim e^{-R_j^2/2R_G^2}$. The two- and three-pion BEC functions of the static granular source can be expressed as [43, 44]

$$C_2(\mathbf{p}_1, \mathbf{p}_2) = 1 + \frac{1}{n} e^{-\mathbf{q}_{12}^2 r_d^2} + \left(1 - \frac{1}{n}\right) e^{-\mathbf{q}_{12}^2 (r_d^2 + R_G^2)} \equiv 1 + \frac{1}{n} \mathcal{R}^d(1, 2) + \left(1 - \frac{1}{n}\right) \mathcal{R}^G(1, 2), \quad (1)$$

$$\begin{aligned} C_3(\mathbf{p}_1, \mathbf{p}_2, \mathbf{p}_3) = & 1 + \frac{1}{n} \left[\mathcal{R}^d(1, 2) + \mathcal{R}^d(1, 3) + \mathcal{R}^d(2, 3) \right] + \left(1 - \frac{1}{n}\right) \left[\mathcal{R}^G(1, 2) + \mathcal{R}^G(1, 3) + \mathcal{R}^G(2, 3) \right] \\ & + \frac{2}{n^2} \left[\mathcal{R}^d(1, 2) \mathcal{R}^d(1, 3) \mathcal{R}^d(2, 3) \right]^{\frac{1}{2}} + \frac{2(n-1)}{n^2} \left[\left(\mathcal{R}^d(1, 3) \mathcal{R}^d(2, 3) / \mathcal{R}^d(1, 2) \right)^{\frac{1}{2}} \mathcal{R}^G(1, 2) \right. \\ & + \left(\mathcal{R}^d(1, 2) \mathcal{R}^d(2, 3) / \mathcal{R}^d(1, 3) \right)^{\frac{1}{2}} \mathcal{R}^G(1, 3) + \left. \left(\mathcal{R}^d(1, 2) \mathcal{R}^d(1, 3) / \mathcal{R}^d(2, 3) \right)^{\frac{1}{2}} \mathcal{R}^G(2, 3) \right] \\ & + \frac{2(n-1)(n-2)}{n^2} \left[\mathcal{R}^G(1, 2) \mathcal{R}^G(1, 3) \mathcal{R}^G(2, 3) \right]^{\frac{1}{2}}, \end{aligned} \quad (2)$$

where n is the droplet number in the granular source, $\mathcal{R}^d(1, 2) = e^{-\mathbf{q}_{12}^2 r_d^2}$, $\mathcal{R}^G(1, 2) = e^{-\mathbf{q}_{12}^2 (r_d^2 + R_G^2)}$, and $\mathbf{q}_{ij} = \mathbf{p}_i - \mathbf{p}_j$ ($i, j = 1, 2, 3, 4$). In Eq. (1), the $\mathcal{R}^d(1, 2)$ and $\mathcal{R}^G(1, 2)$ terms express the correlations of two pions emitted from one droplet and different droplets, respectively. In Eq. (2), the $\frac{2}{n^2}[\dots]$ and $\frac{2(n-1)}{n^2}[\dots]$ terms express the pure triplet correlations of three pions emitted from one droplet and two pions emitted from one droplet, respectively. In Eq. (2), the last term expresses the pure triplet correlations of three pions emitted from different droplets. The two- and three-pion correlation functions become those of the Gaussian sources when

$n \rightarrow \infty$ ($r_d \rightarrow 0$). Similarly, one can get the four-pion correlation function of the static granular source as given in Appendix A.

For a small droplet radius, the pion emission from a droplet is significantly coherent [10, 11, 41, 42]. Assuming the pions emitted from one droplet are completely coherent, the two- and three-pion correlation functions of the granular source become

$$C_2(\mathbf{p}_1, \mathbf{p}_2) = 1 + \frac{(n-1)}{n} \mathcal{R}^G(1, 2), \quad (3)$$

$$C_3(\mathbf{p}_1, \mathbf{p}_2, \mathbf{p}_3) = 1 + \frac{(n-1)}{n} \left[\mathcal{R}^G(1, 2) + \mathcal{R}^G(1, 3) + \mathcal{R}^G(2, 3) \right] + \frac{2(n-1)(n-2)}{n^2} \left[\mathcal{R}^G(1, 2) \mathcal{R}^G(1, 3) \mathcal{R}^G(2, 3) \right]^{\frac{1}{2}}. \quad (4)$$

The four-pion correlation function of the granular source with completely coherent pion-emission droplets can be expressed as

$$\begin{aligned} C_4(\mathbf{p}_1, \mathbf{p}_2, \mathbf{p}_3, \mathbf{p}_4) = & 1 + \frac{(n-1)}{n} \left[\mathcal{R}^G(1, 2) + \mathcal{R}^G(1, 3) + \mathcal{R}^G(1, 4) + \mathcal{R}^G(2, 3) + \mathcal{R}^G(2, 4) + \mathcal{R}^G(3, 4) \right] \\ & + \frac{2(n-1)(n-2)}{n^2} \left[\left(\mathcal{R}^G(1, 2) \mathcal{R}^G(1, 3) \mathcal{R}^G(2, 3) \right)^{\frac{1}{2}} + \left(\mathcal{R}^G(1, 2) \mathcal{R}^G(1, 4) \mathcal{R}^G(2, 4) \right)^{\frac{1}{2}} \right. \\ & + \left. \left(\mathcal{R}^G(2, 3) \mathcal{R}^G(2, 4) \mathcal{R}^G(3, 4) \right)^{\frac{1}{2}} + \left(\mathcal{R}^G(1, 3) \mathcal{R}^G(1, 4) \mathcal{R}^G(3, 4) \right)^{\frac{1}{2}} \right] \end{aligned}$$

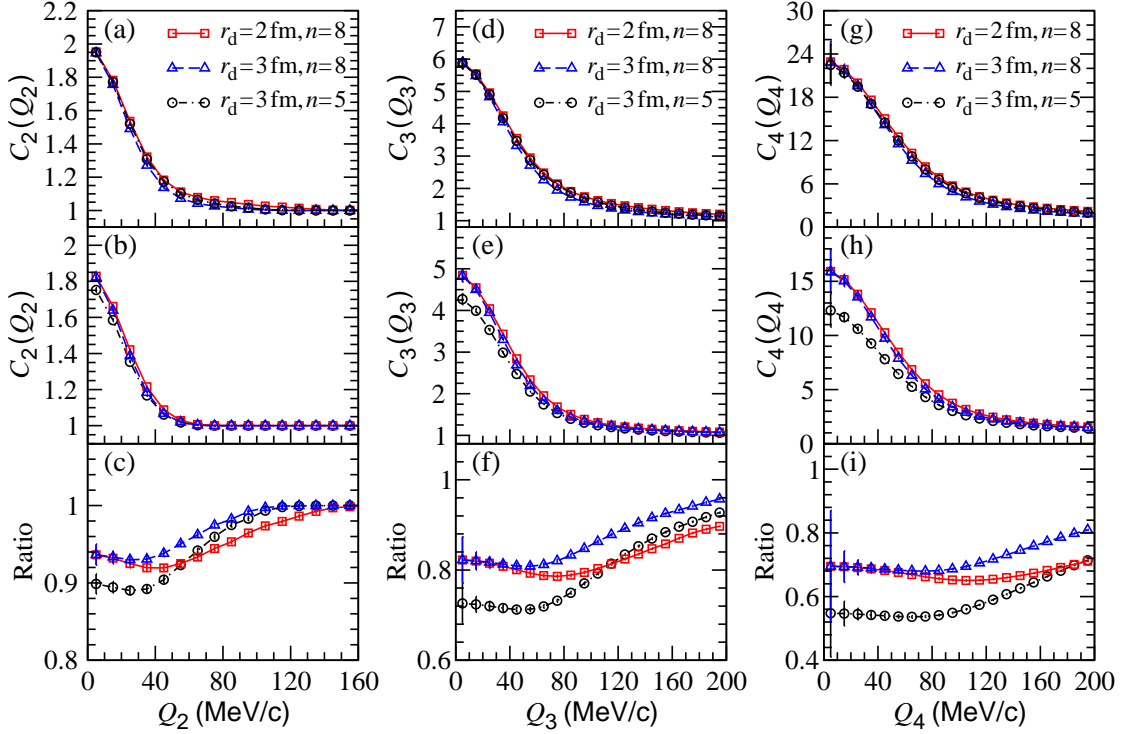


FIG. 1: (Color online) Two-, three- and four-pion correlation functions of the static granular source with chaotic (top panels) and completely coherent (middle panels) pion-emission droplets. Here, the radii of the granular sources are taken to be $R_G = 6.0$ fm. The bottom panels are the ratios of the correlation functions of the granular sources with the completely coherent droplets to the granular sources with the chaotic droplets.

$$\begin{aligned}
& + \frac{(n-1)(n-2)(n-3)}{n^3} \left[\mathcal{R}^G(1,2)\mathcal{R}^G(3,4) + \mathcal{R}^G(1,3)\mathcal{R}^G(2,4) + \mathcal{R}^G(2,3)\mathcal{R}^G(1,4) \right] \\
& + \frac{(n-1)}{n^3} \left[\mathcal{R}^G(1,2)\mathcal{R}^G(3,4) \left(e^{-2\mathbf{q}_{12} \cdot \mathbf{q}_{34} R_G^2} + e^{-2\mathbf{q}_{12} \cdot \mathbf{q}_{43} R_G^2} \right) + \mathcal{R}^G(1,3)\mathcal{R}^G(2,4) \right. \\
& \quad \times \left(e^{-2\mathbf{q}_{13} \cdot \mathbf{q}_{24} R_G^2} + e^{-2\mathbf{q}_{13} \cdot \mathbf{q}_{42} R_G^2} \right) + \mathcal{R}^G(1,4)\mathcal{R}^G(2,3) \left(e^{-2\mathbf{q}_{14} \cdot \mathbf{q}_{23} R_G^2} + e^{-2\mathbf{q}_{14} \cdot \mathbf{q}_{32} R_G^2} \right) \left. \right] \\
& + \frac{2(n-1)(n-2)}{n^3} \left[\mathcal{R}^G(1,2)\mathcal{R}^G(3,4) \left(e^{-\mathbf{q}_{12} \cdot \mathbf{q}_{34} R_G^2} + e^{-\mathbf{q}_{12} \cdot \mathbf{q}_{43} R_G^2} \right) + \mathcal{R}^G(1,3)\mathcal{R}^G(2,4) \right. \\
& \quad \times \left(e^{-\mathbf{q}_{13} \cdot \mathbf{q}_{24} R_G^2} + e^{-\mathbf{q}_{13} \cdot \mathbf{q}_{42} R_G^2} \right) + \mathcal{R}^G(1,4)\mathcal{R}^G(2,3) \left(e^{-\mathbf{q}_{14} \cdot \mathbf{q}_{23} R_G^2} + e^{-\mathbf{q}_{14} \cdot \mathbf{q}_{32} R_G^2} \right) \left. \right] \\
& + \frac{2(n-1)(n-2)(n-3)}{n^3} \left[\left(\mathcal{R}^G(1,2)\mathcal{R}^G(2,3)\mathcal{R}^G(3,4)\mathcal{R}^G(1,4) \right)^{\frac{1}{2}} \right. \\
& \quad + \left(\mathcal{R}^G(1,3)\mathcal{R}^G(2,3)\mathcal{R}^G(2,4)\mathcal{R}^G(1,4) \right)^{\frac{1}{2}} + \left. \left(\mathcal{R}^G(1,2)\mathcal{R}^G(2,4)\mathcal{R}^G(3,4)\mathcal{R}^G(1,3) \right)^{\frac{1}{2}} \right], \quad (5)
\end{aligned}$$

where the third square brackets are the correlations of double pion pairs where four pions are emitted from four different droplets; the fourth square brackets are the correlations of double pion pairs where the two pions of a pair are emitted from two different droplets and the two pions of another pair are emitted respectively from the two droplets also; the fifth square brackets are the correlations of double pion pairs where the two pions of a pair are emitted from two different droplets and the two

pions of another pair are emitted respectively from one of the same droplets and from another droplet; and the last square brackets are the pure quadruplet pion correlations where four pions emitted from different four droplets. A detailed deviation of the correlation function may see in Appendix A.

In Figs. 1(a) and 1(b), we plot the two-pion correlation functions of the static granular sources with chaotic and completely coherent pion-emission droplets, respectively.

In Figs. 1(d) and 1(e), we plot the three-pion correlation functions of the static granular sources with chaotic and completely coherent pion-emission droplets, respectively. In Figs. 1(g) and 1(h), we plot the four-pion correlation functions of the static granular sources with chaotic and completely coherent pion-emission droplets, respectively. The panels (c), (f) and (i) show the ratios of the correlation functions of the granular sources with completely coherent pion-emission droplets to the correlation functions of the granular source with chaotic pion-emission droplets. Here, the radii of the granular sources are taken to be $R_G = 6.0$ fm. The variable Q_m ($m = 2, 3, \dots$) is defined by the covariant relative momenta, as

$$Q_m = \sqrt{\sum_{i < j \leq m} -(p_i - p_j)^\mu (p_i - p_j)_\mu}, \quad (m \geq 2). \quad (6)$$

From Fig. 1 it can be seen that the intercepts of the correlation functions of the granular sources with the completely coherent droplets decrease obviously compared with the granular sources with the chaotic droplets. The intercept decreases will become small with increasing droplet number n . The intercept of the four-pion correlation function decreases much than those of two- and three-pion correlation functions for a fixed droplet number n . From the ratio results one can see that the correlation functions for the completely coherent droplets have the more decreases for a small droplet radius in the high relative-momentum variable regions.

The normalized three-pion correlation function r_3 is defined by the ratio of the three-pion cumulant correlator to the square root of the product of the two-particle correlators [20]. For the granular source with completely coherent pion-emission droplets, it is given by

$$r_3(Q_3) = \frac{[c_3(Q_3) - 1][n/(n-1)]^{3/2}}{\sqrt{\mathcal{R}^G(1,2)(Q_3)\mathcal{R}^G(2,3)(Q_3)\mathcal{R}^G(1,3)(Q_3)}}, \quad (7)$$

where

$$c_3(Q_3) = 1 + \frac{2(n-1)(n-2)}{n^2} \times \left[\mathcal{R}^G(1,2)\mathcal{R}^G(1,3)\mathcal{R}^G(2,3) \right]^{\frac{1}{2}}(Q_3). \quad (8)$$

Because r_3 is insensitive to resonance decay, it is used to measure source coherence in analyses of experimental data [7, 22–24]. Similarly, the normalized four-pion correlation function r_4 of the granular source is given by

$$r_4(Q_4) = \frac{[c_4(Q_4) - 1][n/(n-1)]^2}{\sqrt{\mathcal{R}^G(1,2)(Q_4)\mathcal{R}^G(2,3)(Q_4)\mathcal{R}^G(3,4)(Q_4)\mathcal{R}^G(1,4)(Q_4)}}, \quad (9)$$

where

$$c_4(Q_4) = 1 + \frac{2(n-1)(n-2)(n-3)}{n^3}$$

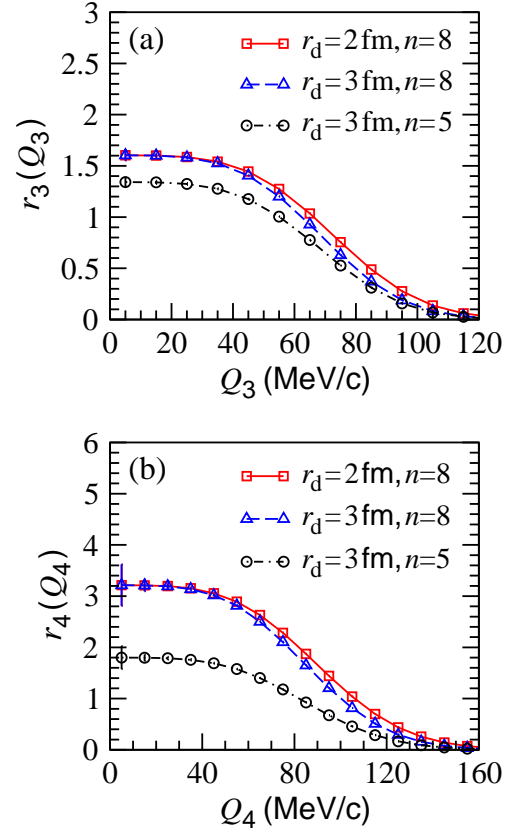


FIG. 2: (Color online) (a) Normalized three-pion correlation functions of the static granular sources with completely coherent pion-emission droplets. (b) Normalized four-pion correlation functions of the static granular sources with completely coherent pion-emission droplets. Parameters of the granular sources are the same as in Fig. 1.

$$\begin{aligned} & \times \left[\left(\mathcal{R}^G(1,2)\mathcal{R}^G(2,3)\mathcal{R}^G(3,4)\mathcal{R}^G(1,4) \right)^{\frac{1}{2}}(Q_4) \right. \\ & + \left(\mathcal{R}^G(1,3)\mathcal{R}^G(2,3)\mathcal{R}^G(2,4)\mathcal{R}^G(1,4) \right)^{\frac{1}{2}}(Q_4) \\ & \left. + \left(\mathcal{R}^G(1,2)\mathcal{R}^G(2,4)\mathcal{R}^G(3,4)\mathcal{R}^G(1,3) \right)^{\frac{1}{2}}(Q_4) \right]. \quad (10) \end{aligned}$$

In Figs. 2(a) and 2(b), we plot the normalized three- and four-pion correlation functions $r_3(Q_3)$ and $r_4(Q_4)$ of the static granular sources with completely coherent pion-emission droplets, respectively. The parameters of the granular source are the same as in Fig. 1. The normalized correlation functions have plateaus in low- $Q_{3,4}$ regions to ~ 50 MeV/c. We plot the intercepts of the $r_3(Q_3)$ and $r_4(Q_4)$ as functions of droplet number in Fig. 3. The intercepts of four-pion normalized correlation functions are more sensitive to the droplet number n than three-pion normalized correlation functions in the $5 < n < 12$ region.

Because without expansion, the three- and four-pion correlation functions of static granular sources fall rapidly with the multi-pion relative momenta Q_3 and Q_4 ,

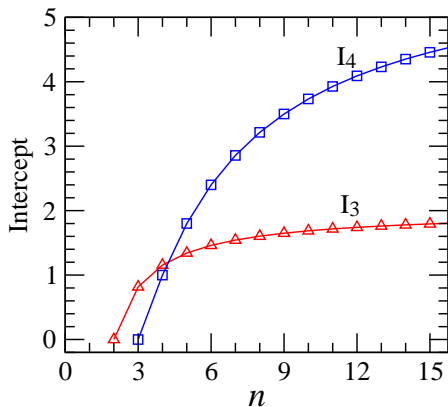


FIG. 3: (Color online) Intercepts of the $r_3(Q_3)$ and $r_4(Q_4)$ of granular sources with completely coherent pion-emission droplets, as functions of droplet number in static granular sources.

respectively. It is hard to describe the experimental data of multi-pion correlations with a static granular source model. We shall investigate in next section the three- and four-pion correlation functions in an evolving granular source model and compare the multi-pion correlation functions with experimental data.

III. MULTI-PION BECS IN EVOLVING GRANULAR SOURCE MODEL

The evolving granular source models can reproduce the pion transverse-momentum spectrum, elliptic flow, and interferometry radii [34–36]. We next investigate the multi-pion BECs for the evolving granular sources in which the droplets expand in viscous hydrodynamics and emit pions coherently.

A. Evolving granular source model

The model we consider is based on a viscous granular source model developed in Ref. [36], but here the pions emitted from one droplet are assumed to be completely or partially coherent. In this subsection, we briefly present the ingredients of the granular source model used in the work. For details of granular source models, the reader is referred to Refs. [28–30, 34–36].

The granular source model was proposed by W. N. Zhang *et al.* [27, 28], to explain the RHIC HBT puzzle, $R_{\text{out}}/R_{\text{side}} \sim 1$ [31, 32, 37, 38], where R_{out} and R_{side} are two HBT radii in transverse plane along and perpendicular to the transverse momentum of the particle pairs [39, 40]. Because the HBT radius R_{out} decrease with decreasing system lifetime and the HBT R_{side} increase with increasing system size, a particle-emitting source with small hot droplets, therefore small evolution time, and distributed in a large space range may lead to a result

of $R_{\text{out}}/R_{\text{side}} \sim 1$ [27–30]. Although the early idea of constructing a granular source model was based on the first-order QCD transition, the occurrence of granular sources may not be limited to first-order phase transition. In relativistic heavy ion collisions at the RHIC and LHC energies, the large system initial fluctuations and some instabilities in the early violent expansion of the system may lead to the granular inhomogeneous structure of the particle-emitting sources [28–30].

In the granular source model, it is assumed that the initial spatial inhomogeneous and violent expansion at the early stages of the system produced in ultrarelativistic heavy-ion collisions may lead to a breakup of the system to many hot and dense droplets and formation of a granular particle-emitting source. At the formation time of the initial granular source, the droplet centers distribute within a cylinder along the collision axis, and the initial energy distribution in a droplet satisfies a Woods-Saxon distribution as in Refs. [35, 36]. The average droplet number, $\langle n \rangle$, of the granular source is related to the initial mean separation and geometry of the source [43].

The evolution of the granular source includes the droplet evolution in viscous hydrodynamics and the droplet expansion in whole with anisotropic droplet velocities v_{dx} , v_{dy} , and v_{dz} . In the granular source model, the geometry and velocity parameters are determined by comparing the model results of pion transverse-momentum spectrum, elliptic flow, and two-pion interferometry radii with experimental data. In this paper, we use the viscous granular source model developed in Ref. [36] to describe the source evolution in Pb-Pb collisions at $\sqrt{s_{NN}} = 2.76$ TeV [8], and the model parameters are taken as the same in [36].

B. Multi-pion correlation functions

In Figs. 4(a) and 4(b), we plot the three-pion correlation functions $C_3(Q_3)$ of the evolving granular sources with completely coherent pion-emission droplets for central Pb-Pb collisions at $\sqrt{s_{NN}} = 2.76$ TeV. The experimental data of $C_3(Q_3)$ measured by the ALICE Collaboration in central Pb-Pb collisions [8] are presented for comparison. Panels (a) and (b) show the results in the low- and high-transverse-momentum intervals $0.16 < K_{T3} < 0.3$ GeV/c and $0.3 < K_{T3} < 1$ GeV/c, respectively. Here, $K_{T3} = |\mathbf{p}_{T1} + \mathbf{p}_{T2} + \mathbf{p}_{T3}|/3$. The average droplet number $\langle n \rangle$ for the simulation events with the granular source parameters determined together by the experimental data of transverse-momentum spectra, elliptic flow, and interferometry radii in 0%–10% Pb-Pb collisions [36] is 8. In Fig. 4, the results for $\langle n \rangle = 9$ and $\langle n \rangle = 6$ are calculated with the same granular source parameters but a smaller and larger initial mean separation. The granular source results in the small- Q_3 region increase with increasing average droplet number $\langle n \rangle$. However, the results for $\langle n \rangle = 8$ are lower than the experimental data in the small- Q_3 region.

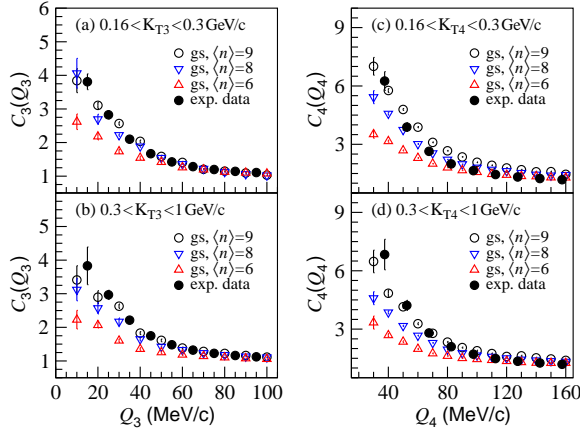


FIG. 4: (Color online) Three- and four-pion correlation functions of evolving granular sources with the completely coherent droplets and experimental data in central Pb-Pb collisions at $\sqrt{s_{NN}} = 2.76$ TeV [8], in transverse-momentum intervals $0.16 < K_{T3} < 0.3$ GeV/c and $0.3 < K_{T3} < 1$ GeV/c. Here, $\langle n \rangle$ denotes average droplet number in evolving granular sources.

In Fig. 4(c) and 4(d), we plot the four-pion correlation functions $C_4(Q_4)$ of the evolving granular sources with completely coherent pion-emission droplets for central Pb-Pb collisions at $\sqrt{s_{NN}} = 2.76$ TeV. The experimental data of $C_4(Q_4)$ measured by the ALICE Collaboration in central Pb-Pb collisions [8] are presented for comparison. Panels (a) and (b) show the results in the low and high transverse-momentum intervals $0.16 < K_{T4} < 0.3$ GeV/c and $0.3 < K_{T4} < 1$ GeV/c, respectively. Here, $K_{T4} = |\mathbf{p}_{T1} + \mathbf{p}_{T2} + \mathbf{p}_{T3} + \mathbf{p}_{T4}|/4$. The four-pion correlation functions of the granular sources increase with increasing average droplet number $\langle n \rangle$ in the small- Q_4 region. In addition, the results for $\langle n \rangle = 8$ are lower than the experimental data in the small- Q_4 region. The multi-pion correlation functions are sensitive to the droplet number in the granular source. However, the transverse-momentum spectrum and elliptic flow of the granular sources are insensitive to $\langle n \rangle$ [34–36].

Considering that the pions with high momenta are more possibly emitted chaotically from the excited states [10, 11, 41, 42], we further investigate the multi-pion BECs for the granular sources with partially coherent pion-emission droplets. We assume that the pions emitted from one droplet and with momenta lower than a fixed value p' are amplitude coherent and therefore without intensity correlation. However, the pions with momenta higher than p' are chaotic emission (from excited-states).

In Figs. 5(a) and 5(b), we compare the three-pion correlation functions of the evolving granular sources with completely coherent pion-emission droplets (corresponding to $p' = \infty$) and partially coherent pion-emission droplets with $p' = 0.5$ and 0.7 GeV/c, in the lower- and higher- transverse-momentum K_{T3} intervals, respectively. Here, the average droplet number of the granular sources is 8 and the solid-circle symbols are the experimental data in central Pb-Pb collisions at $\sqrt{s_{NN}} = 2.76$ TeV [8].

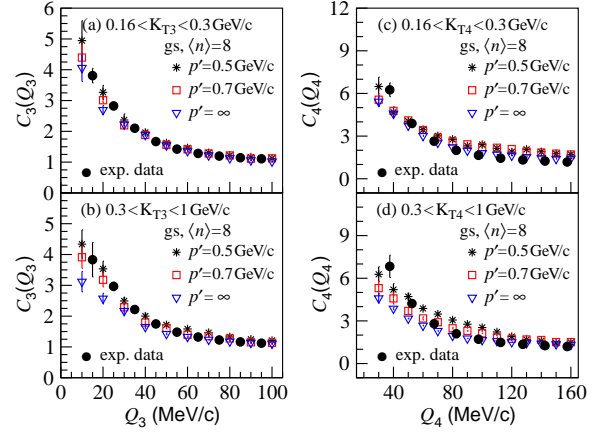


FIG. 5: (Color online) Three- and four-pion correlation functions of evolving granular sources with completely coherent ($p' = \infty$) and partially coherent ($p' = 0.5$ and 0.7 GeV/c) pion-emission droplets, in transverse-momentum intervals $0.16 < K_{T3} < 0.3$ GeV/c and $0.3 < K_{T3} < 1$ GeV/c. Here, average droplet number of the granular source is 8 and solid-circle symbols are experimental data in central Pb-Pb collisions at $\sqrt{s_{NN}} = 2.76$ TeV [8].

mental data in central Pb-Pb collisions at $\sqrt{s_{NN}} = 2.76$ TeV [8]. In the low- Q_3 region, the three-pion correlation functions exhibit an increase with decreasing p' and the increase is greater in the higher K_{T3} interval than in the lower K_{T3} interval. This is because the contribution of chaotic pion emission in the correlation functions increases with decreasing p' and the pions with high momenta, which are more possibly emitted chaotically, have higher K_{T3} than those with low momenta. The three-pion correlation functions of the granular source with $p' = 0.5$ GeV/c are approximately in agreement with the experimental data.

In Figs. 5(c) and 5(d), we compare the four-pion correlation functions of the evolving granular sources with completely coherent pion-emission droplets (corresponding to $p' = \infty$) and partially coherent pion-emission droplets with $p' = 0.5$ and 0.7 GeV/c, in the lower- and higher-transverse-momentum K_{T4} intervals, respectively. Here, the average droplet number of the granular sources is 8 and the solid-circle symbols are the experimental data in central Pb-Pb collisions at $\sqrt{s_{NN}} = 2.76$ TeV [8]. Compared with the three-pion correlation functions, the four-pion correlation functions of the granular source are more sensitive to the value of p' , but inconsistent with the experimental data. This puzzle in the current framework indicates that more considerations of the partially coherent pion-emission are needed to let the model multi-pion correlation functions agree with experimental data.

C. Normalized multi-pion BEC functions

The normalized multi-pion correlation functions r_3 and r_4 are believed to be suitable for analyzing the source co-

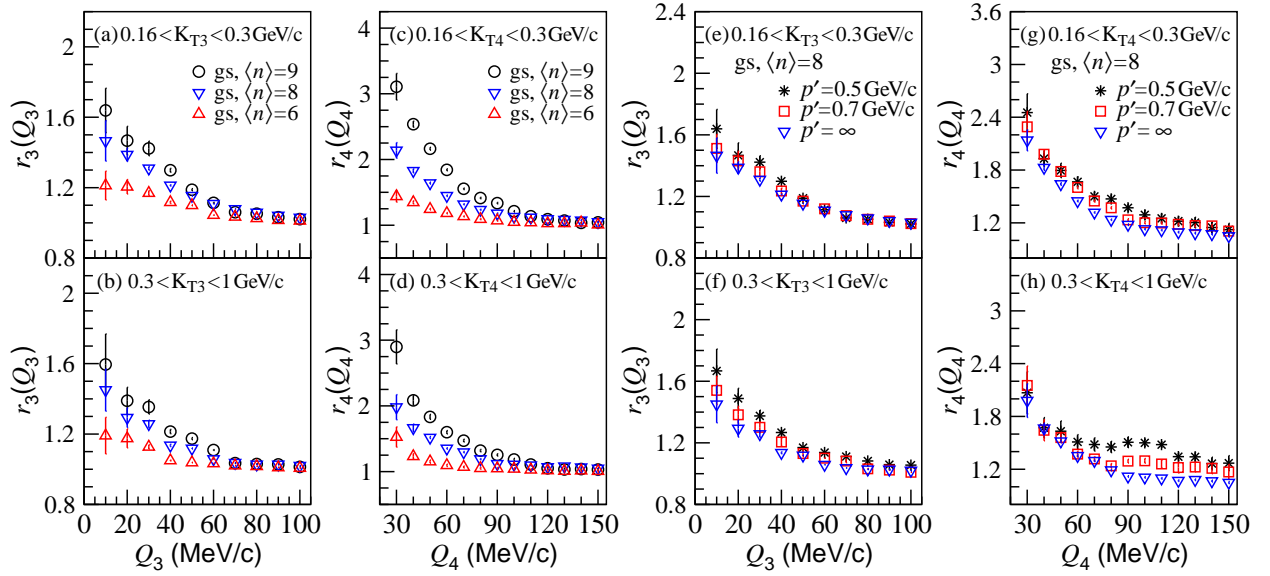


FIG. 6: (Color online) (a) – (d) Normalized three- and four-pion correlation functions of evolving granular sources with completely coherent pion-emission droplets. (e) – (h) Normalized three and four-pion correlation functions of evolving granular sources with partially coherent ($p' = 0.5$ and 0.7 GeV/c) and completely coherent ($p' = \infty$) pion-emission droplets for the average droplet number $\langle n \rangle = 8$.

herence in relativistic heavy-ion collisions. In the preceding section, it was found that the normalized correlation functions are sensitive to droplet number in the static granular source with completely coherent pion-emission droplets. In this subsection, we investigate r_3 and r_4 in the evolving granular source with completely coherent and partially coherent pion-emission droplets.

We show in Figs. 6(a) and 6(b) the normalized three-pion correlation functions of the evolving granular sources with completely coherent pion-emission droplets and the different values of average droplet number $\langle n \rangle$ in the transverse-momentum intervals $0.16 < K_{T3} < 0.3$ GeV/c and $0.3 < K_{T3} < 1$ GeV/c, respectively. The normalized correlation function increases with increasing $\langle n \rangle$ in both transverse-momentum intervals. Compared with the normalized three-pion correlation functions of the static granular sources shown in Fig. 2(a), which have a plateau structure in the small- Q_3 region, the results of the evolving granular sources with the large $\langle n \rangle$ values decrease with Q_3 in the small- Q_3 region. The decrease of r_3 with increasing Q_3 indicates that the three-pion cumulant correlator (correlation of pure pion-triplet interference) decreases more rapidly with increasing Q_3 than two-pion correlations.

We show in Figs. 6(c) and 6(d) the normalized four-pion correlation functions of the evolving granular sources with completely coherent pion-emission droplets and the different values of average droplet number $\langle n \rangle$ in the transverse-momentum intervals $0.16 < K_{T4} < 0.3$ GeV/c and $0.3 < K_{T4} < 1$ GeV/c, respectively. The normalized correlation function increases with increasing $\langle n \rangle$ in both transverse-momentum intervals. Compared with the normalized three-pion correlation functions of

the evolving granular sources, the four-pion correlation functions are more sensitive to $\langle n \rangle$.

In Figs. 6(e) – 6(h), we compare the normalized three- and four-pion correlation functions of the evolving granular sources with completely coherent ($p' = \infty$) and partially coherent ($p' = 0.5$ and 0.7 GeV/c) pion-emission droplets. Here, the average droplet number in the granular source is 8. The normalized three-pion correlation functions increase slightly with decreasing p' . However, the intercepts of the correlation functions at $Q_3 \sim 0$ are approximately in agreement, because the intercept is mainly determined by the droplet number in the granular source. The normalized four-pion correlation functions increase with decreasing p' . In the wide transverse-momentum interval, $0.3 < K_{T4} < 1$ GeV/c, the normalized four-pion correlation function for the smallest p' has an obvious enhancement at approximately $Q_4 \sim 100$ MeV/c due to the momentum dependence of pion-emission coherence and the sensitivity of high-order pion correlations to source coherence. As discussed in Ref. [11], the average pion momentum will increase with increasing Q_4 if there are no other constraints. This leads to an increase of chaotic emission possibility with increasing Q_4 and the enhancement of $r_4(Q_4)$ in the middle- Q_4 region [see Fig. 7(d) in [11]]. It is related to that the high-momentum pions are more possibly emitted chaotically from excited states.

Table I presents the results of $r_3(Q_3)$ and $r_4(Q_4)$ at $Q_3 = 10$ MeV/c and $Q_4 = 30$ MeV/c, respectively, for the partially coherent pion emissions from a droplet with $p' = 0.5$ GeV/c, $p' = 0.7$ GeV/c, and $p' = \infty$. One can see that the intercept results are almost consistent within the errors.

TABLE I: Results of $r_3(Q_3=10\text{MeV}/c)$ and $r_4(Q_4=30\text{MeV}/c)$ for the partially coherent pion emissions of droplet with $p'=0.5\text{GeV}/c$, $p'=0.7\text{GeV}/c$, and $p'=\infty$.

$p'(\text{GeV}/c)$	0.5	0.7	∞
$r_3(Q_3=10\text{MeV}/c)$			
$0.16 < K_{T3} < 0.3 \text{ GeV}/c$	1.64 ± 0.13	1.51 ± 0.10	1.47 ± 0.11
$0.3 < K_{T3} < 1 \text{ GeV}/c$	1.67 ± 0.14	1.54 ± 0.10	1.45 ± 0.12
$r_4(Q_4=30\text{MeV}/c)$			
$0.16 < K_{T4} < 0.3 \text{ GeV}/c$	2.45 ± 0.21	2.29 ± 0.18	2.14 ± 0.12
$0.3 < K_{T4} < 1 \text{ GeV}/c$	2.07 ± 0.24	2.15 ± 0.22	1.98 ± 0.19

IV. SUMMARY AND DISCUSSION

We investigate the three- and four-pion BECs in the granular source model with coherent pion-emission droplets. The three- and four-pion correlation functions and the normalized multi-pion correlation functions of the granular sources are examined for completely coherent and momentum-dependent partially coherent pion-emissions from a droplet. It is found that the intercepts of the multi-pion correlation functions at the relative momenta near zero are sensitive to droplet number in the granular source. They decrease with decreasing droplet number.

By comparing the three- and four-pion correlation functions of evolving granular sources with the experimental data in Pb-Pb collisions at $\sqrt{s_{NN}} = 2.76 \text{ TeV}$ at the LHC, we find that the three-pion correlation functions for the evolving granular sources with momentum-dependent partially coherent pion-emission droplets are in basic agreement with the experimental data in the transverse-momentum intervals $0.16 < K_{T3} < 0.3 \text{ GeV}/c$ and $0.3 < K_{T3} < 1 \text{ GeV}/c$. However, the model results of four-pion correlation function are inconsistent with the experimental data. To solve the puzzle of the multi-pion correlation functions, one needs more consideration of the coherent pion emission. For instance, the coherent emission may not only be dependent on particle momentum magnitude but also be particle-azimuthal-angle dependent. Figures. 5(c) and 5(d) show that the model results in the higher-transverse-momentum K_{T4} interval have more enhancements compared to the experimental data than those in the lower-transverse-momentum K_{T4} intervals. This may indicate that the pions with small relative azimuthal angles, thus larger K_{T4} , are possibly a coherent emission, though they have momenta higher than the value of p' . The four-particle correlations are sensitive to the coherent emission and should be investigated in more detail in model and experimental data analyses.

The normalized multi-pion correlation functions, defined as the ratios of the multi-pion cumulant correlators to the two-pion correlator, can reduce the influence of resonance decay on themselves. Our investigations indicate that the normalized four-pion correlation function has an obvious enhancement in $Q_4 \sim 100\text{-MeV}/c$ region for the wide transverse momentum interval $0.3 < K_{T4} < 1 \text{ GeV}/c$. It is related to that the high-momentum pions are more possibly emitted chaotically from excited states.

Recently, D. Gangadharan proposed a technique of constructing three- and four-pion correlation functions for partially coherent sources and estimating the source coherence [9]. Using this technique the ALICE Collaboration analyzed the three- and four-pion correlation functions in Pb-Pb collisions at $\sqrt{s_{NN}} = 2.76 \text{ TeV}$ at the LHC [8]. They find that the source coherent fraction extracted from the four-pion correlation function cannot explain the data of three-pion correlation function if the sources are assumed partially coherent [8]. How to consistently solve the suppressions of the three- and four-pion BECs in a partially coherent source model is still an open question.

Finally, it should be mentioned that the granular source model used in this paper had the same model parameters as Ref. [36], but with the assumption of coherent pion emission from one droplet. We noted that this assumption may increase the two-pion interferometry radii by $\sim 4\%$ on average and decrease the two-pion chaoticity parameter λ by $\sim 10\%$. However, the assumption of coherent pion emission hardly changes the results of the transverse-momentum spectrum and elliptic flow. Considering more realistic pion coherent emission, using the Gangadharan's technique to granular source, and investigating multi-pion BECs in more realistic model will be of interest.

Acknowledgments

This research was supported by the National Natural Science Foundation of China under Grant Nos. 11675034 and 11275037.

Appendix A: Expression of four-pion correlation function of static granular source

With the formulism developed in Refs. [43, 44], one can get the four-pion correlation function of the static granular source with completely chaotic pion emission droplets as

$$\begin{aligned}
& + e^{-(\mathbf{q}_{14}^2 + \mathbf{q}_{23}^2)R_G^2/2} e^{-(\mathbf{q}_{14} + \mathbf{q}_{32})^2 R_G^2/2} \Big) + e^{-(\mathbf{q}_{12}^2 + \mathbf{q}_{24}^2 + \mathbf{q}_{43}^2 + \mathbf{q}_{31}^2)r_d^2/2} \Big(e^{-(\mathbf{q}_{12}^2 + \mathbf{q}_{13}^2 + \mathbf{q}_{23}^2)R_G^2/2} \\
& + e^{-(\mathbf{q}_{12}^2 + \mathbf{q}_{14}^2 + \mathbf{q}_{24}^2)R_G^2/2} + e^{-(\mathbf{q}_{13}^2 + \mathbf{q}_{14}^2 + \mathbf{q}_{34}^2)R_G^2/2} + e^{-(\mathbf{q}_{23}^2 + \mathbf{q}_{24}^2 + \mathbf{q}_{34}^2)R_G^2/2} \\
& + e^{-(\mathbf{q}_{13}^2 + \mathbf{q}_{24}^2)R_G^2/2} e^{-(\mathbf{q}_{13} + \mathbf{q}_{42})^2 R_G^2/2} + e^{-(\mathbf{q}_{12}^2 + \mathbf{q}_{34}^2)R_G^2/2} e^{-(\mathbf{q}_{12} + \mathbf{q}_{43})^2 R_G^2/2} \Big) \\
& + e^{-(\mathbf{q}_{13}^2 + \mathbf{q}_{32}^2 + \mathbf{q}_{24}^2 + \mathbf{q}_{41}^2)r_d^2/2} \Big(e^{-(\mathbf{q}_{12}^2 + \mathbf{q}_{13}^2 + \mathbf{q}_{23}^2)R_G^2/2} + e^{-(\mathbf{q}_{12}^2 + \mathbf{q}_{14}^2 + \mathbf{q}_{24}^2)R_G^2/2} \\
& + e^{-(\mathbf{q}_{13}^2 + \mathbf{q}_{14}^2 + \mathbf{q}_{34}^2)R_G^2/2} + e^{-(\mathbf{q}_{23}^2 + \mathbf{q}_{24}^2 + \mathbf{q}_{34}^2)R_G^2/2} + e^{-(\mathbf{q}_{13}^2 + \mathbf{q}_{24}^2)R_G^2/2} e^{-(\mathbf{q}_{13} + \mathbf{q}_{42})^2 R_G^2/2} \\
& + e^{-(\mathbf{q}_{14}^2 + \mathbf{q}_{23}^2)R_G^2/2} e^{-(\mathbf{q}_{14} + \mathbf{q}_{32})^2 R_G^2/2} \Big) \Big], \tag{A1}
\end{aligned}$$

where $\mathbf{q}_{ij} = \mathbf{p}_i - \mathbf{p}_j$ ($i, j = 1, 2, 3, 4$) and n is the droplet number in the granular source. In Eq. (A1), the first and second square brackets are the correlations of two pions which are emitted from one droplet and from two different droplets, respectively; the third and forth square brackets are the pure triplet correlations of three pions which are emitted from one droplet and from three different droplets, respectively; the fifth square brackets are the pure triplet correlations of three pions where two pions are emitted from one droplet and another pion is emitted from a different droplet; the sixth and seventh square brackets are the correlations of double pion pairs where each pair is emitted from one droplet and the four pions are emitted from four different droplets, respectively; the eighth square brackets are the correlations of double pion pairs where one pion pair is emitted from one droplet and the two pions of another pair are emitted from two different droplets; the ninth square brackets are the correlations of double pion pairs where the two pions of a pair are emitted from two different droplets and the two pions of another pair are emitted respectively from the two droplets also; the tenth square brackets are the correlations of double pion pairs where the two pions of a pair are emitted from two different droplets and the two pions of another pair are emitted respectively from one of the same droplets and from another droplet; the eleventh and twelfth square brackets are the pure quadruplet correlations of four pions emitted from one droplet and from

four different droplets, respectively; the thirteenth square brackets are the pure quadruplet correlations of four pions where three pions are emitted from one droplet and another pion is emitted from a different droplet; the fourteenth square brackets are the pure quadruplet correlations of four pions where two pions are emitted from one droplet and the other two pions are emitted from another droplet; and finally, the fifteenth square brackets are the pure quadruplet correlations of four pions where two pions are emitted from one droplet and the other two pions are respectively emitted from two different droplets.

The four-pion correlation function of granular source is complex which includes the relative angles of two relative momenta in the double pair correlations and pure quadruplet correlations. For the completely chaotic pion emission droplet, $C_4(\mathbf{p}_1, \mathbf{p}_2, \mathbf{p}_3, \mathbf{p}_4) = 24$ when $\mathbf{q}_{ij} = 0$ ($i, j = 1, 2, 3, 4$). For a partially coherent pion-emission from a droplet, if the coherent emission in a droplet have the same Gaussian distribution of the chaotic pion emission and with a constant ratio of coherent emission contribution b_c to chaotic emission contribution b_χ , $\gamma = b_c/b_\chi$, the terms of two, pure triplet, double pair, and pure quadruplet pion correlations will reduce by the factors [12, 45], $\lambda = (1 + 2\gamma)/(1 + \gamma)^2$, $\xi = (1 + 3\gamma)/(1 + \gamma)^3$, λ^2 , and $\eta = (1 + 4\gamma)/(1 + \gamma)^4$, respectively. In this case, the four-pion correlation function of the granular source with partially coherent pion-emission droplets is given by,

$$\begin{aligned}
C_4(\mathbf{p}_1, \mathbf{p}_2, \mathbf{p}_3, \mathbf{p}_4) = 1 & + \frac{\lambda}{n} \left[e^{-\mathbf{q}_{12}^2 r_d^2} + e^{-\mathbf{q}_{13}^2 r_d^2} + e^{-\mathbf{q}_{14}^2 r_d^2} + e^{-\mathbf{q}_{23}^2 r_d^2} + e^{-\mathbf{q}_{24}^2 r_d^2} + e^{-\mathbf{q}_{34}^2 r_d^2} \right] + \frac{(n-1)}{n} \left[e^{-\mathbf{q}_{12}^2 (r_d^2 + R_G^2)} \right. \\
& + e^{-\mathbf{q}_{13}^2 (r_d^2 + R_G^2)} + e^{-\mathbf{q}_{14}^2 (r_d^2 + R_G^2)} + e^{-\mathbf{q}_{23}^2 (r_d^2 + R_G^2)} + e^{-\mathbf{q}_{24}^2 (r_d^2 + R_G^2)} + e^{-\mathbf{q}_{34}^2 (r_d^2 + R_G^2)} \Big] \\
& + \frac{2\xi}{n^2} \left[e^{-(\mathbf{q}_{12}^2 + \mathbf{q}_{13}^2 + \mathbf{q}_{23}^2)r_d^2/2} + e^{-(\mathbf{q}_{12}^2 + \mathbf{q}_{14}^2 + \mathbf{q}_{24}^2)r_d^2/2} + e^{-(\mathbf{q}_{13}^2 + \mathbf{q}_{14}^2 + \mathbf{q}_{34}^2)r_d^2/2} + e^{-(\mathbf{q}_{23}^2 + \mathbf{q}_{24}^2 + \mathbf{q}_{34}^2)r_d^2/2} \right] \\
& + \frac{2(n-1)(n-2)}{n^2} \left[e^{-(\mathbf{q}_{12}^2 + \mathbf{q}_{13}^2 + \mathbf{q}_{23}^2)(r_d^2 + R_G^2)/2} + e^{-(\mathbf{q}_{12}^2 + \mathbf{q}_{14}^2 + \mathbf{q}_{24}^2)(r_d^2 + R_G^2)/2} \right. \\
& + e^{-(\mathbf{q}_{13}^2 + \mathbf{q}_{14}^2 + \mathbf{q}_{34}^2)(r_d^2 + R_G^2)/2} + e^{-(\mathbf{q}_{23}^2 + \mathbf{q}_{24}^2 + \mathbf{q}_{34}^2)(r_d^2 + R_G^2)/2} \Big] \\
& + \frac{2(n-1)\lambda}{n^2} \left[e^{-(\mathbf{q}_{12}^2 + \mathbf{q}_{13}^2 + \mathbf{q}_{23}^2)r_d^2/2} \left(e^{-\mathbf{q}_{12}^2 R_G^2} + e^{-\mathbf{q}_{13}^2 R_G^2} + e^{-\mathbf{q}_{23}^2 R_G^2} \right) + e^{-(\mathbf{q}_{12}^2 + \mathbf{q}_{14}^2 + \mathbf{q}_{24}^2)r_d^2/2} \right. \\
& \times \left(e^{-\mathbf{q}_{12}^2 R_G^2} + e^{-\mathbf{q}_{14}^2 R_G^2} + e^{-\mathbf{q}_{24}^2 R_G^2} \right) + e^{-(\mathbf{q}_{13}^2 + \mathbf{q}_{14}^2 + \mathbf{q}_{34}^2)r_d^2/2} \left(e^{-\mathbf{q}_{13}^2 R_G^2} + e^{-\mathbf{q}_{14}^2 R_G^2} + e^{-\mathbf{q}_{34}^2 R_G^2} \right) \Big]
\end{aligned}$$

$$\begin{aligned}
& + e^{-(\mathbf{q}_{23}^2 + \mathbf{q}_{24}^2 + \mathbf{q}_{34}^2)r_d^2/2} \left(e^{-\mathbf{q}_{23}^2 R_G^2} + e^{-\mathbf{q}_{24}^2 R_G^2} + e^{-\mathbf{q}_{34}^2 R_G^2} \right) \Big] + \frac{\lambda^2}{n^2} \left[e^{-(\mathbf{q}_{12}^2 + \mathbf{q}_{34}^2)r_d^2} \right. \\
& + e^{-(\mathbf{q}_{13}^2 + \mathbf{q}_{24}^2)r_d^2} + e^{-(\mathbf{q}_{14}^2 + \mathbf{q}_{23}^2)r_d^2} \Big] + \frac{(n-1)(n-2)(n-3)}{n^3} \left[e^{-(\mathbf{q}_{12}^2 + \mathbf{q}_{34}^2)(r_d^2 + R_G^2)} \right. \\
& + e^{-(\mathbf{q}_{13}^2 + \mathbf{q}_{24}^2)(r_d^2 + R_G^2)} + e^{-(\mathbf{q}_{14}^2 + \mathbf{q}_{23}^2)(r_d^2 + R_G^2)} \Big] + \frac{(n-1)\lambda}{n^2} \left[e^{-\mathbf{q}_{12}^2 r_d^2} e^{-\mathbf{q}_{34}^2 (r_d^2 + R_G^2)} \right. \\
& + e^{-\mathbf{q}_{13}^2 r_d^2} e^{-\mathbf{q}_{24}^2 (r_d^2 + R_G^2)} + e^{-\mathbf{q}_{14}^2 r_d^2} e^{-\mathbf{q}_{23}^2 (r_d^2 + R_G^2)} + e^{-\mathbf{q}_{23}^2 r_d^2} e^{-\mathbf{q}_{14}^2 (r_d^2 + R_G^2)} + e^{-\mathbf{q}_{24}^2 r_d^2} e^{-\mathbf{q}_{13}^2 (r_d^2 + R_G^2)} \\
& + e^{-\mathbf{q}_{34}^2 r_d^2} e^{-\mathbf{q}_{12}^2 (r_d^2 + R_G^2)} \Big] + \frac{(n-1)}{n^3} \left[e^{-(\mathbf{q}_{12}^2 + \mathbf{q}_{34}^2)r_d^2} e^{-(\mathbf{q}_{12} + \mathbf{q}_{34})^2 R_G^2} + e^{-(\mathbf{q}_{12}^2 + \mathbf{q}_{34}^2)r_d^2} \right. \\
& \times e^{-(\mathbf{q}_{12} + \mathbf{q}_{43})^2 R_G^2} + e^{-(\mathbf{q}_{13}^2 + \mathbf{q}_{24}^2)r_d^2} e^{-(\mathbf{q}_{13} + \mathbf{q}_{24})^2 R_G^2} + e^{-(\mathbf{q}_{13}^2 + \mathbf{q}_{24}^2)r_d^2} e^{-(\mathbf{q}_{13} + \mathbf{q}_{42})^2 R_G^2} \\
& + e^{-(\mathbf{q}_{14}^2 + \mathbf{q}_{23}^2)r_d^2} e^{-(\mathbf{q}_{14} + \mathbf{q}_{23})^2 R_G^2} + e^{-(\mathbf{q}_{14}^2 + \mathbf{q}_{23}^2)r_d^2} e^{-(\mathbf{q}_{14} + \mathbf{q}_{32})^2 R_G^2} \Big] \\
& + \frac{2(n-1)(n-2)}{n^3} \left[e^{-(\mathbf{q}_{12}^2 + \mathbf{q}_{34}^2)r_d^2} e^{-(\mathbf{q}_{12}^2 + \mathbf{q}_{34}^2)R_G^2/2} \left(e^{-(\mathbf{q}_{12} + \mathbf{q}_{34})^2 R_G^2/2} + e^{-(\mathbf{q}_{12} + \mathbf{q}_{43})^2 R_G^2/2} \right) \right. \\
& + e^{-(\mathbf{q}_{13}^2 + \mathbf{q}_{24}^2)r_d^2} e^{-(\mathbf{q}_{13}^2 + \mathbf{q}_{24}^2)R_G^2/2} \left(e^{-(\mathbf{q}_{13} + \mathbf{q}_{24})^2 R_G^2/2} + e^{-(\mathbf{q}_{13} + \mathbf{q}_{42})^2 R_G^2/2} \right) \\
& + e^{-(\mathbf{q}_{14}^2 + \mathbf{q}_{23}^2)r_d^2} e^{-(\mathbf{q}_{14}^2 + \mathbf{q}_{23}^2)R_G^2/2} \left(e^{-(\mathbf{q}_{14} + \mathbf{q}_{23})^2 R_G^2/2} + e^{-(\mathbf{q}_{14} + \mathbf{q}_{32})^2 R_G^2/2} \right) \Big] \\
& + \frac{2\eta}{n^3} \left[e^{-(\mathbf{q}_{12}^2 + \mathbf{q}_{23}^2 + \mathbf{q}_{34}^2 + \mathbf{q}_{41}^2)r_d^2/2} + e^{-(\mathbf{q}_{12}^2 + \mathbf{q}_{24}^2 + \mathbf{q}_{43}^2 + \mathbf{q}_{31}^2)r_d^2/2} + e^{-(\mathbf{q}_{13}^2 + \mathbf{q}_{32}^2 + \mathbf{q}_{24}^2 + \mathbf{q}_{41}^2)r_d^2/2} \right] \\
& + \frac{2(n-1)(n-2)(n-3)}{n^3} \left[e^{-(\mathbf{q}_{12}^2 + \mathbf{q}_{23}^2 + \mathbf{q}_{34}^2 + \mathbf{q}_{41}^2)(r_d^2 + R_G^2)/2} + e^{-(\mathbf{q}_{12}^2 + \mathbf{q}_{24}^2 + \mathbf{q}_{43}^2 + \mathbf{q}_{31}^2)(r_d^2 + R_G^2)/2} \right. \\
& + e^{-(\mathbf{q}_{13}^2 + \mathbf{q}_{32}^2 + \mathbf{q}_{24}^2 + \mathbf{q}_{41}^2)(r_d^2 + R_G^2)/2} \Big] + \frac{2(n-1)\xi}{n^3} \left[e^{-(\mathbf{q}_{12}^2 + \mathbf{q}_{23}^2 + \mathbf{q}_{34}^2 + \mathbf{q}_{41}^2)r_d^2/2} \left(e^{-\mathbf{q}_{12}^2 R_G^2} \right. \right. \\
& + e^{-\mathbf{q}_{23}^2 R_G^2} + e^{-\mathbf{q}_{34}^2 R_G^2} + e^{-\mathbf{q}_{41}^2 R_G^2} \Big) + e^{-(\mathbf{q}_{12}^2 + \mathbf{q}_{24}^2 + \mathbf{q}_{43}^2 + \mathbf{q}_{31}^2)r_d^2/2} \left(e^{-\mathbf{q}_{12}^2 R_G^2} + e^{-\mathbf{q}_{24}^2 R_G^2} \right. \\
& + e^{-\mathbf{q}_{43}^2 R_G^2} + e^{-\mathbf{q}_{31}^2 R_G^2} \Big) + e^{-(\mathbf{q}_{13}^2 + \mathbf{q}_{32}^2 + \mathbf{q}_{24}^2 + \mathbf{q}_{41}^2)r_d^2/2} \left(e^{-\mathbf{q}_{13}^2 R_G^2} + e^{-\mathbf{q}_{32}^2 R_G^2} + e^{-\mathbf{q}_{24}^2 R_G^2} + e^{-\mathbf{q}_{41}^2 R_G^2} \right) \Big] \\
& + \frac{(n-1)\lambda^2}{n^3} \left[e^{-(\mathbf{q}_{12}^2 + \mathbf{q}_{23}^2 + \mathbf{q}_{34}^2 + \mathbf{q}_{41}^2)r_d^2/2} \left(e^{-(\mathbf{q}_{12} + \mathbf{q}_{23})^2 R_G^2} + e^{-(\mathbf{q}_{12} + \mathbf{q}_{34})^2 R_G^2} + e^{-(\mathbf{q}_{12} + \mathbf{q}_{41})^2 R_G^2} \right. \right. \\
& + e^{-(\mathbf{q}_{23} + \mathbf{q}_{34})^2 R_G^2} + e^{-(\mathbf{q}_{23} + \mathbf{q}_{41})^2 R_G^2} + e^{-(\mathbf{q}_{34} + \mathbf{q}_{41})^2 R_G^2} \Big) + e^{-(\mathbf{q}_{12}^2 + \mathbf{q}_{24}^2 + \mathbf{q}_{43}^2 + \mathbf{q}_{31}^2)r_d^2/2} \\
& \times \left(e^{-(\mathbf{q}_{12} + \mathbf{q}_{24})^2 R_G^2} + e^{-(\mathbf{q}_{12} + \mathbf{q}_{43})^2 R_G^2} + e^{-(\mathbf{q}_{12} + \mathbf{q}_{31})^2 R_G^2} + e^{-(\mathbf{q}_{24} + \mathbf{q}_{43})^2 R_G^2} + e^{-(\mathbf{q}_{24} + \mathbf{q}_{31})^2 R_G^2} \right. \\
& + e^{-(\mathbf{q}_{43} + \mathbf{q}_{31})^2 R_G^2} \Big) + e^{-(\mathbf{q}_{13}^2 + \mathbf{q}_{32}^2 + \mathbf{q}_{24}^2 + \mathbf{q}_{41}^2)r_d^2/2} \left(e^{-(\mathbf{q}_{13} + \mathbf{q}_{32})^2 R_G^2} + e^{-(\mathbf{q}_{13} + \mathbf{q}_{24})^2 R_G^2} \right. \\
& + e^{-(\mathbf{q}_{13} + \mathbf{q}_{41})^2 R_G^2} + e^{-(\mathbf{q}_{32} + \mathbf{q}_{24})^2 R_G^2} + e^{-(\mathbf{q}_{32} + \mathbf{q}_{41})^2 R_G^2} + e^{-(\mathbf{q}_{24} + \mathbf{q}_{41})^2 R_G^2} \Big) \Big] \\
& + \frac{2(n-1)(n-2)\lambda}{n^3} \left[e^{-(\mathbf{q}_{12}^2 + \mathbf{q}_{23}^2 + \mathbf{q}_{34}^2 + \mathbf{q}_{41}^2)r_d^2/2} \left(e^{-(\mathbf{q}_{12}^2 + \mathbf{q}_{13}^2 + \mathbf{q}_{23}^2)R_G^2/2} + e^{-(\mathbf{q}_{12}^2 + \mathbf{q}_{14}^2 + \mathbf{q}_{24}^2)R_G^2/2} \right. \right. \\
& + e^{-(\mathbf{q}_{13}^2 + \mathbf{q}_{14}^2 + \mathbf{q}_{34}^2)R_G^2/2} + e^{-(\mathbf{q}_{23}^2 + \mathbf{q}_{24}^2 + \mathbf{q}_{34}^2)R_G^2/2} + e^{-(\mathbf{q}_{12}^2 + \mathbf{q}_{34}^2)R_G^2/2} e^{-(\mathbf{q}_{12} + \mathbf{q}_{43})^2 R_G^2/2} \\
& + e^{-(\mathbf{q}_{14}^2 + \mathbf{q}_{23}^2)R_G^2/2} e^{-(\mathbf{q}_{14} + \mathbf{q}_{32})^2 R_G^2/2} \Big) + e^{-(\mathbf{q}_{12}^2 + \mathbf{q}_{24}^2 + \mathbf{q}_{43}^2 + \mathbf{q}_{31}^2)r_d^2/2} \left(e^{-(\mathbf{q}_{12}^2 + \mathbf{q}_{13}^2 + \mathbf{q}_{23}^2)R_G^2/2} \right. \\
& + e^{-(\mathbf{q}_{12}^2 + \mathbf{q}_{14}^2 + \mathbf{q}_{24}^2)R_G^2/2} + e^{-(\mathbf{q}_{13}^2 + \mathbf{q}_{14}^2 + \mathbf{q}_{34}^2)R_G^2/2} + e^{-(\mathbf{q}_{23}^2 + \mathbf{q}_{24}^2 + \mathbf{q}_{34}^2)R_G^2/2} \\
& + e^{-(\mathbf{q}_{13}^2 + \mathbf{q}_{24}^2)R_G^2/2} e^{-(\mathbf{q}_{13} + \mathbf{q}_{42})^2 R_G^2/2} + e^{-(\mathbf{q}_{12}^2 + \mathbf{q}_{34}^2)R_G^2/2} e^{-(\mathbf{q}_{12} + \mathbf{q}_{43})^2 R_G^2/2} \Big) \\
& + e^{-(\mathbf{q}_{13}^2 + \mathbf{q}_{32}^2 + \mathbf{q}_{24}^2 + \mathbf{q}_{41}^2)r_d^2/2} \left(e^{-(\mathbf{q}_{12}^2 + \mathbf{q}_{13}^2 + \mathbf{q}_{23}^2)R_G^2/2} + e^{-(\mathbf{q}_{12}^2 + \mathbf{q}_{14}^2 + \mathbf{q}_{24}^2)R_G^2/2} \right. \\
& + e^{-(\mathbf{q}_{13}^2 + \mathbf{q}_{14}^2 + \mathbf{q}_{34}^2)R_G^2/2} + e^{-(\mathbf{q}_{23}^2 + \mathbf{q}_{24}^2 + \mathbf{q}_{34}^2)R_G^2/2} + e^{-(\mathbf{q}_{13}^2 + \mathbf{q}_{24}^2)R_G^2/2} e^{-(\mathbf{q}_{13} + \mathbf{q}_{42})^2 R_G^2/2} \\
& + e^{-(\mathbf{q}_{14}^2 + \mathbf{q}_{23}^2)R_G^2/2} e^{-(\mathbf{q}_{14} + \mathbf{q}_{32})^2 R_G^2/2} \Big) \Big], \tag{A2}
\end{aligned}$$

For the granular source with completely coherent pion-emission droplets, the factors λ , ξ , and η are zero, and the four-pion correlation function reduces to a simple

formula [see Eq. (5)]. In this case, the maximum of $C_4(\mathbf{p}_1, \mathbf{p}_2, \mathbf{p}_3, \mathbf{p}_4)$ at $\mathbf{q}_{ij} = 0$ ($i, j = 1, 2, 3, 4$) is n -dependent.

-
- [1] M. Gyulassy, S. K. Kauffmann, and Lance W. Wilson, Phys. Rev. C **20**, 2267 (1979).
- [2] C. Y. Wong, *Introduction to High-Energy Heavy-Ion Collisions* (World Scientific, Singapore, 1994), Chap. 17.
- [3] U. A. Wienemann and U. Heinz, Phys. Rep. **319**, 145 (1999).
- [4] R. M. Weiner, Phys. Rep. **327**, 249 (2000).
- [5] T. Csörgő, Heavy Ion Physics **15** (2002) 1; arXiv:hep-ph/0001233.
- [6] M. A. Lisa, S. Pratt, R. Soltz, and U. Wiedemann, Annu. Rev. Nucl. Part. Sci. **55**, 357 (2005).
- [7] B. Abelev et al. (ALICE Collaboration), Phys. Rev. C **89** (2014) 024911.
- [8] J. Adam et al. (ALICE Collaboration), Phys. Rev. C **93** (2016) 054908.
- [9] D. Gangadharan, Phys. Rev. C **92** (2015) 014902.
- [10] G. Bary, P. Ru, and W. N. Zhang, J. Phys. G **45** (2018) 065102.
- [11] G. Bary, P. Ru, and W. N. Zhang, J. Phys. G **46** (2019) 115107.
- [12] Y. M. Liu, D. Beavis, S. Y. Chu, S. Y. Fung, D. Keane, G. VanDalen, and M. Vient, Phys. Rev. C **34** (1986) 1667.
- [13] W. A. Zajc, Phys. Rev. **D35**, (1987) 3396.
- [14] M. Biyajima, A. Bartl, T. Mizoguchi, N. Suzuki and O. Terazawa, Prog. Theor. Phys. **84** (1990) 931.
- [15] I. V. Andreev, M. Plümer, R. M. Weiner, Phys. Rev. Lett. **67**, (1991) 3475; I. V. Andreev, M. Plümer, R. M. Weiner, Int. J. Mod. Phys. **A8**, (1993) 4577.
- [16] S. Pratt, Phys. Lett. B **301** (1993) 159.
- [17] T. Csörgő and J. Zimányi, Phys. Rev. Lett. **80** (1998) 916; J. Zimányi and T. Csörgő, Heavy Ion Physics **9** (1999) 241; arXiv:hep-ph/9705432.
- [18] W. N. Zhang, Y. M. Liu, S. Wang *et al.*, Phys. Rev. **C47**, (1993) 795; W. N. Zhang, Y. M. Liu, L. Huo *et al.*, Phys. Rev. **C51**, (1995) 922; W. N. Zhang, L. Huo, X. J. Chen *et al.*, Phys. Rev. **C58**, (1998) 2311; W. N. Zhang, G. X. Tang, X. J. Chen *et al.*, Phys. Rev. **C62**, (2000) 044903.
- [19] W. Q. Chao, C. S. Gao, and Q. H. Zhang, J. Phys. **G21**, (1995) 847; Q. H. Zhang, W. Q. Chao, and C. S. Gao, Phys. Rev. **C52**, (1995) 2064.
- [20] U. Heinz and Q. H. Zhang, Phys. Rev. C **56** (1997) 426; U. Heinz and A. Sugarbaker, Phys. Rev. C **70** (2004) 054908.
- [21] H. Nakamura and R. Seki, Phys. Rev. **C60**, (1999) 064904; H. Nakamura and R. Seki, Phys. Rev. **C61**, (2000) 054905.
- [22] H. Bøggild et al. (NA44 Collaboration), Phys. Lett. B **455** (1999) 77; I. G. Bearden et al. (NA44 Collaboration), Phys. Lett. B **517** (2001) 25.
- [23] M. M. Aggarwa et al. (WA98 Collaboration), Phys. Rev. Lett. **85** (2000) 2895;
- M. M. Aggarwa et al. (WA98 Collaboration), Phys. Rev. C **67** (2003) 014906.
- [24] J. Adams et al. (STAR Collaboration), Phys. Rev. Lett. **91** (2003) 262301.
- [25] M. Csanáda for the PHENIX Collaboration, Nucl. Phys. A **774** (2006) 611.
- [26] K. Morita, S. Muroya, and H. Nakamura, Prog. Theor. Phys. **116** (2006) 329.
- [27] W. N. Zhang, M. J. Efaaf, C. Y. Wong, Phys. Rev. C **70** (2004) 024903.
- [28] W. N. Zhang, Y. Y. Ren, and C. Y. Wong, Phys. Rev. C **74** (2006) 024908.
- [29] W. N. Zhang, Z. T. Yang, and Y. Y. Ren, Phys. Rev. C **80** (2009) 044908.
- [30] W. N. Zhang, H. J. Yin, and Y. Y. Ren, Chin. Phys. Lett. **28** (2011) 122501.
- [31] S. S. Adler *et al.* (PHENIX Collaboration), Phys. Rev. Lett. **93** (2004) 152302.
- [32] J. Adams *et al.* (STAR Collaboration), Phys. Rev. **71** (2005) 044906.
- [33] K. Aamodt *et al.* (ALICE Collaboration), Phys. Lett. B **696** (2011) 328.
- [34] J. Yang, Y. Y. Ren, and W. N. Zhang, Advances in High Energy Physic, **2015** (2015) 846154.
- [35] J. Yang, Y. Y. Ren, and W. N. Zhang, in Proceeding of the Xth Workshop on Particle Correlations and Femtoscopy (WPCF14) (Gyöngyös, Hungary on Aug. 2014); arXiv:1501.03651[nucl-th].
- [36] J. Yang, W. N. Zhang, and Y. Y. Ren, Chinese Physics C **41** (2017) 084102.
- [37] C. Adler *et al.* (STAR Collaboration), Phys. Rev. Lett. **87**, 082301 (2001).
- [38] K. Adcox *et al.* (PHENIX Collaboration), Phys. Rev. Lett. **88**, 192302 (2002).
- [39] G. Bertsch, M. Gong, and M. Tohyama, Phys. Rev. C **37**, 1896 (1988); G. Bertsch, Nucl. Phys. A **498**, 173c (1989).
- [40] S. Pratt, T. Csörgő, and J. Zimányi, Phys. Rev. C **42**, 2646 (1990).
- [41] C. Y. Wong and W. N. Zhang, Phys. Rev. C **76** (2007) 034905.
- [42] J. Liu, P. Ru, W. N. Zhang, C. Y. Wong, J. Phys. G **41** (2014) 125101.
- [43] S. Pratt, P. J. Siemens, and A. P. Vischer, Phys. Rev. Lett. **68** (1992) 1109.
- [44] W. N. Zhang, Y. M. Liu, L. Huo, Y. Z. Jiang, D. Keane, and S. Y. Fung, Phys. Rev. C **51** (1995) 922.
- [45] Y. M. Liu, PhD thesis, University of California, Riverside, 1985.